Cancer Cell Detection and Morphology Analysis Based on Local Interest Point Detectors

Tiago Esteves[1,3], Maria José Oliveira[2,3], and Pedro Quelhas[1,3]

[1] Departamento de Engenharia Electrotécnica e de Computadores,
Faculdade de Engenharia, Universidade do Porto,
Rua Dr. Roberto Frias, 4200-465 Porto, Portugal
[2] Departamento de Patologia e Oncologia,
Faculdade de Medicina da Universidade do Porto,
Alameda Prof. Hernni Monteiro s/n, 420-319 Porto, Portugal
[3] INEB - Instituto de Engenharia Biomédica,
Rua do Campo Alegre, 823, 4150-180 Porto, Portugal
dee11017@fe.up.pt
http://paginas.fe.up.pt/∼dee11017/

Abstract. The automatic analysis of cancer cells has gained increasing relevance given the amount of data that biology researchers have to analyze. However, most biology researchers still analyze cells by visual inspection alone, which is time consuming and prone to induce subjective bias. This makes automatic cell image analysis essential for large scale, objective studies of cells.

While the classic approach for automatic cell detection is to use image segmentation, in the case of *in vivo* brightfield images, such approach is not robust to image quality changes. To detect cells with robustness and increased performance we propose the use of local interest point detectors. We perform a comparison study between the use of the Laplacian of Gaussian filter, a Bank of Ring Filters and local convergence filters.

Based on experimental results we found that the Laplacian of Gaussian filter outperformed all other in cell detection obtaining an accuracy of 78%. Additionally, through the analysis of shape fit, we found that the Laplacian of Gaussian filter obtained a better approximation to the shape of the cells having a Dice's coefficient of 81%.

1 Introduction

The detection of cancer cells is fundamental for the understanding of complex cellular responses which leads to the development of possible therapies for cell's regulation [1,2]. Usually, to study cancer cells dynamics, these are placed on top of native surfaces or of extracellular matrix-coated surfaces and a time lapse video is collected. A typical brightfield frame of an example video can be seen in figure 1(a). While all cancer cells are similar at the beginning of the experiment, their shape changes during the experiment as is visible in figure 1(b). These morphological changes make the automatic cell detection process more difficult.

J.M. Sanches, L. Micó, and J.S. Cardoso (Eds.): IbPRIA 2013, LNCS 7887, pp. 624–631, 2013.
© Springer-Verlag Berlin Heidelberg 2013

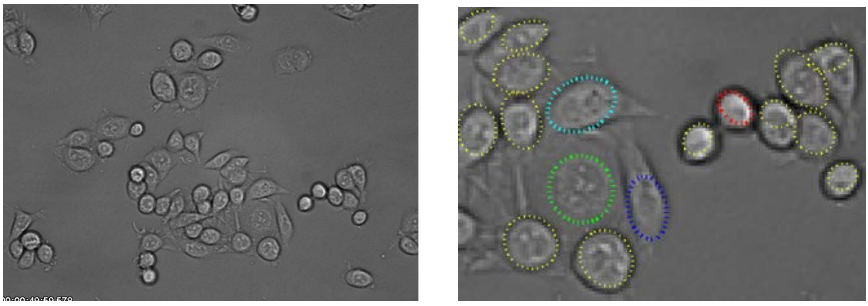

(a) (b)

Fig. 1. Cells on top of an extracellular matrix surface. a) Example of a typical cancer cell time-lapse movie frame; b) Cropped image detailing different cells morphology.

The classical approach to perform cell detection is based on image segmentation, which is a fundamental problem in computer vision [3]. The specific methods for segmentation range from image thresholding [4], in the case of high contrast between cells and background to more advanced methods such as mean-shift clustering. In the case of touching cells, as the spatial relations are not embedded in image levels, watershed transform is widely used [4]. One of the main issues with most automatic image segmentation approaches is that their parameters are not robust to image quality or characteristics variations [3,4]. Additionally, parameters are complex to someone unfamiliar with image processing, requiring experts for readjustments, reducing usability.

Recently local image filters have been introduced to aid in cell detection based on shape. Usaj et al. proposed the use of the Laplacian of Gaussian (LoG) for cell detection in fluorescence images, leading to enhancement and subsequent detection of cell's due to their approximated circular shape [2]. The use of a Bank of ring filter has also been used to perform cell detection in phase contrast microscopy images [5]. Esteves et al. proposed the use of local convergence filters (LCF) for the detection and shape estimation of cell nuclei in fluorescence images [4].

We propose the application of the aforementioned local filters for the task of cancer cell detection in brightfield images in order to perform a comparative study of their performance.

2 Methodology

We propose using local image filters for cell detection. Based on the response of the filter we detect cells by searching for local maxima. For this task we use the LoG filter [6], a ring filter matching approach [5] and LCF [4]. From existing LCFs we selected the Coin filter [7], the Iris filter [7], the Adaptative Ring filter [8] and the Sliding Band filter [4].

In the next subsections we start by introducing the LoG filter for the task of cell detection then the ring filter matching approach is explained and finally the LCF are presented.

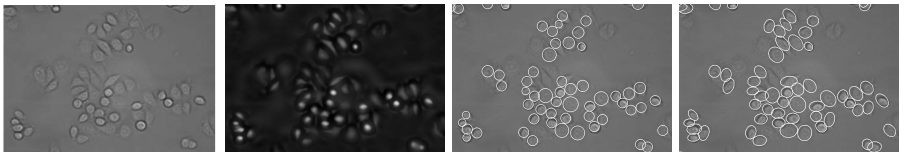

(a) (b) (c) (d)

Fig. 2. LoG based cell detection: a) Brightfield frame with cancer cells; b) LoG response; c) Detections overlaid in the image; d) Cells detections shown as ellipses based on Hessian estimated eccentricity

2.1 LoG Filter

The LoG filter is based on the image scale-space representation to enhance the blob like structure as introduced by Lindeberg [6]. Given an input image $I(x, y)$, the gaussian scale space representation at a certain scale t is:

$$L(x, y, t) = g(x, y, t) * I(x, y), \ \textit{where} \ g(x, y, t) = \frac{1}{2\pi t} e^{\frac{x^2+y^2}{2t}}. \tag{1}$$

The scale normalized LoG operator is then defined as:

$$\nabla^2 L(x, y, t) = t^2 (L_{xx}(x, y, t) + L_{yy}(x, y, t)), \tag{2}$$

where L_{xx} and L_{yy} are the second derivatives of the input image in x and y respectively, and t^2 is the scale normalization parameter.

We set the scale of the filter, t, to the expected range of the cell radius (figure 2(a)). We perform detection of cells by detecting local maxima of LoG response in the input image (figure 2(b)). The detected maxima enable us to estimate the position and radius ($r = 1.5 \times t$) of cells (figure 2(c)).

By using the LoG filter for cell detection there is an underlying assumption of a circular shape. However, this may not be the case, leading to inaccurate shape adaptation. To further refine the cell's shape we use the Hessian matrix:

$$H(x, y, t) = \begin{bmatrix} L_{xx} & L_{xy} \\ L_{yx} & L_{yy} \end{bmatrix}. \tag{3}$$

From the eigenvectors and eigenvalues of H we obtain the orientation and eccentricity values for the respective cells' ellipsoid shape approximation (figure 2(d)) [6].

2.2 Ring Filter Matching

The use of ring filters has also been proposed to detect cells in phase contrast microscopy images which consists of a series of matched filters with multiple-radius ring-shaped templates [5].

The cell detection scheme consists in filtering the input image with a multiple-radius ring filter (figure 3(a)) and locate cell candidate locations through local maxima response [5]. As illustrated in figure 3(b), the highest peak occurs when

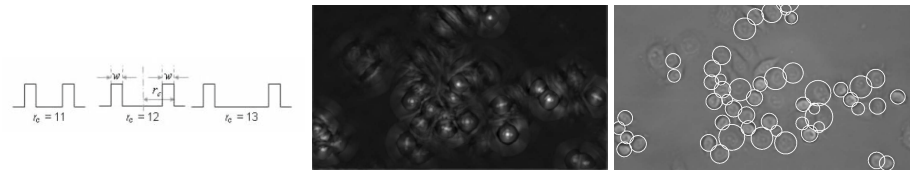

(a) (b) (c)

Fig. 3. Ring filter matching: a) Ring filter bank where rc is the radius and w is the width of the ring; b) Ring filter response from the $figure\ 2(a)$ input image; c) Detections overlaid in the original image

the radius of the filter matches exactly that of the cell pattern, and lower peaks are generated when the filter mismatches slightly. An example of detected cells is shown in figure 3(c).

2.3 Local Convergence Filters

By assuming a convex shape and a limited range of sizes for cell areas we can use LCF for cell detection and shape estimation. This is possible since LCF filters detect local gradient convergence in the image which are usually an indication of cell membrane locations [4].

LCF are based on the maximization of the convergence index (CI) at each image point of spatial coordinates (x, y). The CI within the support region (SR), which is the region that defines each specific filter, is defined using the cosine between the polar direction θ_i and the image gradient for coordinate (x, y, θ_i, m):

$$CI(x, y, i, m) = \cos(\theta_i - \alpha(x, y, \theta_i, m)), \tag{4}$$

where (θ_i, m) are polar coordinates within the filter's SR. The overall convergence is obtained by summing all the individual convergences within the specific SR of each filter.

For cancer dell detection in brightfield images we tested several LCF:

COIN Filter: The COIN filter (CF) assumes a circle with variable radius as SR. The value of the radius is varied in search for maximum convergency [7]. The CF formulation is given by the diagram and formulas in figure 4(a) where r is the radius of the circle of the SR that varies from *0* to R_{max}, N is the number of radial directions for which convergence is evaluated.

The SR of this filter corresponds to N half-lines that radiate from the point (x, y), where we calculate the filter's response. The result of applying CF equation to the input image, is the filter's response image (figure 4(b)). The maxima of such response indicate the locations of interest. For each location we obtain the radius of the SR at that location through the $r_{shape}(x, y)$ equation in figure 4(a), shown in figure 4(c), overlayed on the input image.

Iris Filter: The Iris filter (IF) adapts the radius of its SR for each of the N directions, maximizing convergence for each radial direction independently [7].

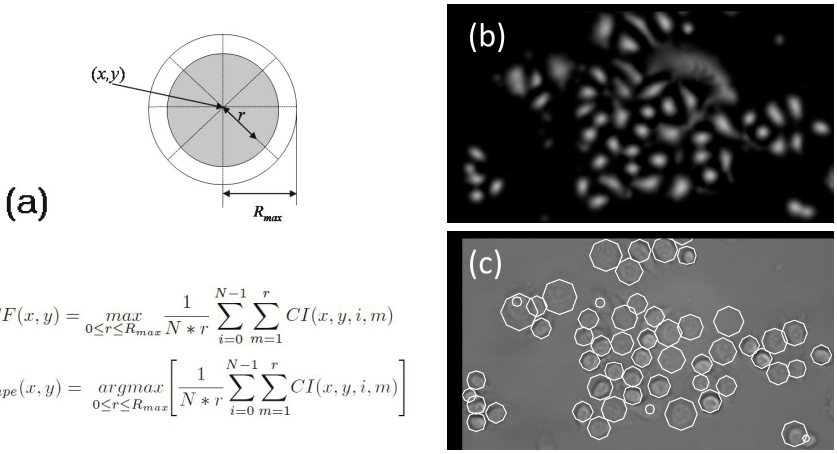

$$CF(x,y) = \max_{0 \le r \le R_{max}} \frac{1}{N * r} \sum_{i=0}^{N-1} \sum_{m=1}^{r} CI(x,y,i,m)$$

$$r_{shape}(x,y) = \underset{0 \le r \le R_{max}}{argmax} \left[\frac{1}{N * r} \sum_{i=0}^{N-1} \sum_{m=1}^{r} CI(x,y,i,m) \right]$$

Fig. 4. COIN filter: a) Schematics of the filter's support region (grey) with N=8; b) CF response from the $figure\ 2(a)$ input image; c) Detections overlaid in the input image

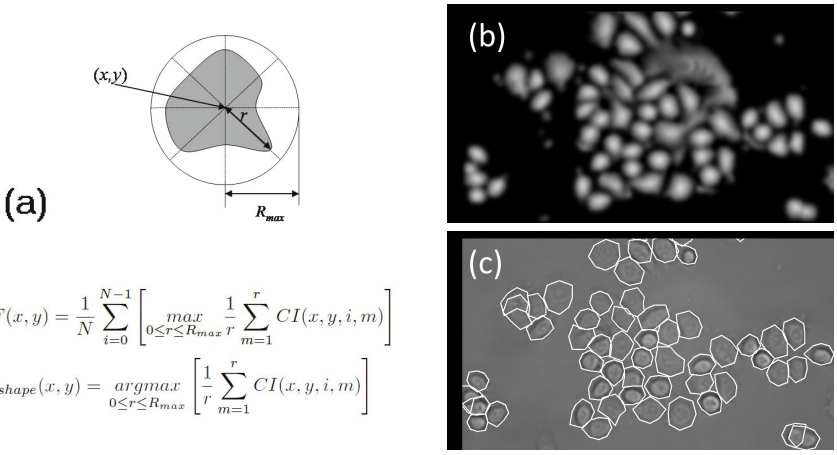

$$IF(x,y) = \frac{1}{N} \sum_{i=0}^{N-1} \left[\max_{0 \le r \le R_{max}} \frac{1}{r} \sum_{m=1}^{r} CI(x,y,i,m) \right]$$

$$r_{shape}(x,y) = \underset{0 \le r \le R_{max}}{argmax} \left[\frac{1}{r} \sum_{m=1}^{r} CI(x,y,i,m) \right]$$

Fig. 5. IRIS filter: a) Schematics of the filter's support region (grey) with N=8; b) IF response from the $figure\ 2(a)$ input image; c) Detections overlaid in the input image

IF is not restricted to circular shapes. Figure 5(a) shows the filter's SR and formulation. While filter maxima still indicate possible object centers, the shape estimation is defined by N independent radii (support points (SP)) equation from figure 5(a). The sets of SP corresponding to the image maxima lead to the shapes detected in the image (figure 5(c)).

Adaptive Ring Filter: The Adaptive Ring Filter (ARF) defines a ring shaped convergence region [8]. The size of the ring used as SR is varied searching for the radius of maximum convergence as given by ARF equation from figure 6(a) where d is the ring width.

Similarly to the process performed when dealing with the CF the shape estimation is performed by searching for the radius of the ring SR for the location

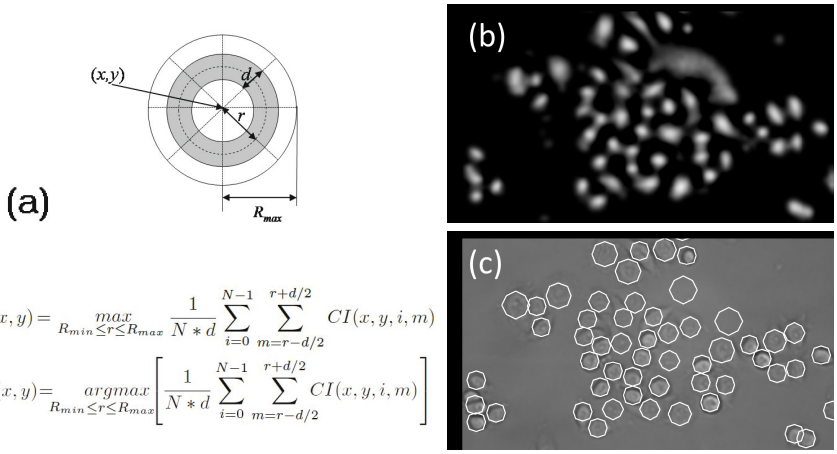

Fig. 6. ARF filter: a) Schematics of the filter's support region (grey) with N=8; b) ARF response from the $figure\ 2(a)$ input image; c) Detections overlaid in the input image

in the image given by equation from figure 6(a). In figure 6(c) we can observe that this filter provides a tighter fit than the CF while having the same final estimated shape (circle).

Sliding Band Filter: The Sliding Band Filter (SBF) combines the ideas of IF and ARF by defining a SR formed by a band of fixed width, with varying radius in each direction to allow for the maximization of the convergence index at each point [4]. The SBF formulation derives from ARF and IF convergence estimation and is given by the SBF equation from figure 7(a) where d corresponds to the width of the band, which is moved between R_{min} and R_{max}. The shape estimation of the SBF filter is similar to that of the IF. This filter combines both the shape flexibility of the IF with the limited band search of the ARF (figure 7(c)).

3 Results and Discussion

To evaluate the performance of the proposed approaches applied for cell detection we tested them on 90 brightfield images from one time lapse video. Each image has in average 70 visible cells and the automatic detection is compared with the respective expert manually labeled ground-truth detection, using several performance measures.

Based on the known scale of the cells in the images we set the parameters for each of the proposed approaches. For the scale normalized LoG filter we set the scale of the filter, t, to the expected range of the cell radius between 4 and 16 pixels. For all LCF analyzed the respective parameters were set based on visual inspection of the cell's shape: $R^n_{min} = 4$; $R^n_{max} = 16$; $q = 4$; $N = 8$ (where applicable).

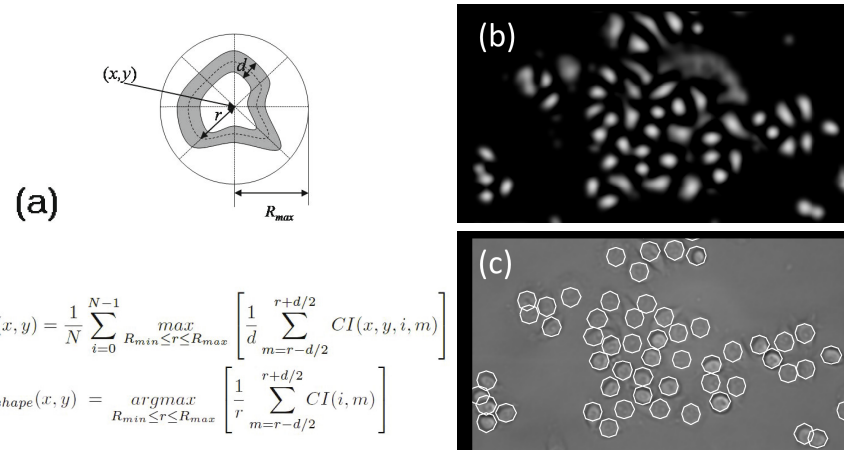

Fig. 7. SBF filter: a) Schematics of the filter's support region (grey) with N=8; b) SBF response from the *figure* 2(*a*) input image; c) Detections overlaid in the input image

Based on the detections and the annotated ground-truth we identify the true positives (TP), false positives (FP) and false negatives (FN) and through the overlap between cell detections and ground-truth areas we measured the Dice's coefficient.

In Table 1 we present the performance results for all methods. From the obtained results we can observe that by using the LoG filter for cell detection we obtained an higher number of TP (58). The Dice's coefficient was also higher using this filter associated with the Hessian based cell shape estimation (0.81) indicating a better estimation of the cell shape using this approach. The use of the ring filter matching approach obtained the worst performance.

Table 1. Cancer cell detection and shape fit performance evaluation. TP - true positives; FP - false positives; FN - false negatives.

Cell detection and Shape fit							
Technique	LoG	LoGHessian	SBF	RFTM	IF	CF	ARF
TP	58	58	55	53	54	55	55
FP	7	7	8	8	8	9	9
FN	9	9	12	14	13	12	12
Accuracy	0.78	0.78	0.73	0.71	0.73	0.72	0.72
Dice's coefficient	0.80	0.81	0.78	0.79	0.78	0.78	0.78

4 Conclusion

We proposed the use of local interest point detector filter for the detection of cancer cells in brightfield time-lapse images. The overall performance of the proposed approaches showed that the LoG filter associated with the ellipse shape

estimation was the one with better performance in cell detection. It was also possible to conclude through the analysis of the shape fit that this approach was able to better estimate the cell shape.

The use of the LoG filter gives us promising results for the automatic detection and shape estimation of cancer cells. In the future work, we plan to perform cell tracking based on this cell detection approach.

Acknowledgements. This work was financed by FEDER funds through the Programa Operacional Factores de Competitividade - COMPETE and by Portuguese funds through FCT - Fundação para a Ciência e a Tecnologia in the framework of the project PEst-C/SAU/LA0002/2011. T. Esteves is recipient of SFRH/BD/80508/2011 by FCT. P. Quelhas is *Ciência2008* awardee.

References

1. Quelhas, P., Marcuzzo, M., Mendonça, A.M., Oliveira, M.J., Campilho, A.: Cancer cell detection and invasion depth estimation in brightfield images. In: BMVC, pp. 1–10 (2009)
2. Usaj, M., Torkar, D., Kanduser, M., Miklavcic, D.: Cell counting tool parameters optimization approach for electroporation efficiency determination of attached cells in phase contrast image. Journal of Microscopy 241(3), 303–314 (2010)
3. Meijering, E.: Cell segmentation: 50 years down the road (life sciences). IEEE Signal Processing Magazine 29(5), 140–145 (2012)
4. Esteves, T., Quelhas, P., Mendonça, A.M., Campilho, A.: Gradient convergence filters for cell nuclei detection: a comparison study with a phase based approach. MVAP 23(4), 623–638 (2012)
5. Eom, S., Bise, R., Kanade, T.: Detection of hematopoietic stem cells in microscopy images using a bank of ring filters. In: 2010 IEEE International Symposium on Biomedical Imaging: From Nano to Macro, pp. 137–140 (April 2010)
6. Lindeberg, T.: Scale-space theory: A basic tool for analyzing structures at different scales. Journal of Applied Statistics 21(2), 224–270 (1994)
7. Kobatake, H., Hashimoto, S.: Convergence index filter for vector fields. IEEE Trans. on Image Processing 8(8), 1029–1038 (1999)
8. Wei, J., Hagihara, Y., Kobatake, H.: Detection of cancerous tumors on chest x-ray images candidate detection filter and its evaluation. In: Proc. of International Conference on Image Analysis and Processing (ICIP), pp. 397–401 (1999)